

PAPER

Fabrication and characterization of bending and pressure sensors for a soft prosthetic hand

To cite this article: Rui Pedro Rocha *et al* 2018 *J. Micromech. Microeng.* **28** 034001

View the [article online](#) for updates and enhancements.

You may also like

- [Properties of TiO₂/PDMS-Ag Composites as Antibacterial Self Cleaning](#)
B P Ardhi, M M Alfin, E Pramono *et al.*
- [Dry adhesives with sensing features](#)
J Krahn and C Menon
- [Microfluidic on CMOS with Laser Cut Adhesive Tape](#)
Akshaya Shanmugam and Christopher D Salthouse



244th Electrochemical Society Meeting

October 8 – 12, 2023 • Gothenburg, Sweden

50 symposia in electrochemistry & solid state science

Abstract submission deadline:
April 7, 2023

Read the call for
papers &
submit your abstract!

Fabrication and characterization of bending and pressure sensors for a soft prosthetic hand

Rui Pedro Rocha¹, Pedro Alhais Lopes¹, Anibal T de Almeida¹,
Mahmoud Tavakoli¹ and Carmel Majidi²

¹ Institute of Systems and Robotics, University of Coimbra, Coimbra, Portugal

² Integrated Soft Materials Lab, Carnegie Mellon University, Pittsburgh, PA 15213, United States of America

E-mail: mahmoud@isr.uc.pt and cmajidi@andrew.cmu.edu

Received 26 August 2017, revised 30 November 2017

Accepted for publication 14 December 2017


Published 17 January 2018



Abstract

We demonstrate fabrication, characterization, and implementation of ‘soft-matter’ pressure and bending sensors for a soft robotic hand. The elastomer-based sensors are embedded in a robot finger composed of a 3D printed endoskeleton and covered by an elastomeric skin. Two types of sensors are evaluated, resistive pressure sensors and capacitive pressure sensors. The sensor is fabricated entirely out of insulating and conductive rubber, the latter composed of polydimethylsiloxane (PDMS) elastomer embedded with a percolating network of structured carbon black (CB). The sensor-integrated fingers have a simple materials architecture, can be fabricated with standard rapid prototyping methods, and are inexpensive to produce. When incorporated into a robotic hand, the CB–PDMS sensors and PDMS carrier medium function as an ‘artificial skin’ for touch and bend detection. Results show improved response with a capacitive sensor architecture, which, unlike a resistive sensor, is robust to electromechanical hysteresis, creep, and drift in the CB–PDMS composite. The sensorized fingers are integrated in an anthropomorphic hand and results for a variety of grasping tasks are presented.

Keywords: soft robotics, conductive elastomer, sensing, robotic hand

 Supplementary material for this article is available [online](#)

(Some figures may appear in colour only in the online journal)

1. Introduction

When grasping objects, the human brain does not control each joint and muscle individually but instead utilizes predefined motion patterns or synergies [1, 2]. Research by Bicchi and Santello suggests that the reason humans are able to grasp a wide variety of objects with a low number of synergies is that the human hand is mechanically compliant and can conform to objects without the need for kinematic precision [3, 4]. Specifically, the compliance of the hand allows several possible contact point postures with a single joint posture. For this reason, soft robotic hands have received increasing attention in recent years. Pisa-IIT SoftHand [5] and its descendant

the SoftHand Pro [6], the ISR-SoftHand [7], the RBO hand 2 [8], and the UB hand [9] are examples of recent development of anthropomorphic hands that directly integrate the compliance into the joints. Flexirigid [10], SDM hands [11, 12] and bio-inspired soft robotic gripper [13] are examples of non anthropomorphic grasping mechanisms that use elastic joints for a better adaptability to objects.

Integration of pressure sensors into the digits of the robotic hand provides useful information for the control system. In the case of prosthetic hands, integration of pressure sensors is a step toward allowing a sense of touch for amputees. Rigid-bodied solutions for sensing pressure may be based on computer vision, optics, or MEMS-based barometer chip. An

example of the latter is the TakkTile sensor array for measuring surface pressure [14]. Although integration of these rigid sensor technologies into a soft robot hand has been demonstrated, it is nonetheless worth exploring the incorporation of fully soft electronics that match the mechanical compliance and elasticity of natural skin. Among the various ‘artificial skin’ sensing architectures, electro-elastostatic transducers composed entirely of insulating and conductive elastomers are attractive because of their skin-like elastic modulus (~ 0.1 – 1 MPa) and high strain limit ($>100\%$). Moreover, because of the simplicity of their design, they can be seamlessly integrated into the fingers of a robot hand using standard rapid prototyping and shape deposition manufacturing (SDM) techniques.

In this article we present the design, integration, characterization and implementation of soft robotic fingers with embedded pressure and bend sensors (figure 1(A)). The goal is an open source hardware architecture that is inexpensive, easy to replicate, and accessible to a broad community of users wishing to create their own customized robot hand prosthetics (figure 1(B)). Similar to the human finger, the soft fingers presented here are composed of a 3D printed endoskeleton that is robust to lateral deflection and twisting loads, as discussed in our previous work [15]. The fingers are integrated with ‘soft-matter’ sensors composed of insulating and conductive elastomer. The conductor is a composite of polydimethylsiloxane (PDMS) ‘silicone’ elastomer embedded with a percolating network of structured carbon black (CB). Referring to figure 1(C), we examine two types of sensors: (i) pressure sensors to measure the applied pressure at the finger tips and (ii) strain sensors that measure the angle of the finger joints. We compare the response of resistive and capacitive sensing architectures for a variety of performance metrics: hysteresis between loading/unloading cycles, response time, and recovery/creep. Grasping tasks are performed with an anthropomorphic soft robot hand containing the sensorized fingers.

2. Background

The field of stretchable electronics and artificial/electronic/robot skin has grown rapidly over the past two decades. It’s progress has been covered in several comprehensive overviews [16–18] and a complete review will not be presented here. Typically, stretchable conductive elements or conductive fluids are incorporated into a soft elastomer. These conductors can range from wavy or serpentine metal wiring [19] to microfluidic channels of liquid metal (LM) gallium–indium alloy [20, 21] and particle-filled elastomer composites. The latter includes elastomers embedded with a percolating network of carbon allotropes (e.g. CB–PDMS) [22, 23], metal microspheres (e.g. Ag–PDMS [24]) and nanoparticles (Ag nanoflakes in soft fluoropolymer [25]), and ionomer groups (PANI–SEBS [26] and PEDOT:PSS–SEBS [27]).

Compared to wavy electronics and LM microfluidics, conductive elastomers are attractive because they do not require deterministic patterning, leak-proof sealing, or specialized

fabrication methods for integration into soft robotic systems. Among the various alternatives for the conductive dispersion phase, carbon black is particularly attractive due to its low cost and ease of processing [28]. In this study, we focus on CB–PDMS composites due to their biocompatibility and well-established electrical and mechanical properties. The conductivity of the percolating CB network is postulated to be a combination of direct physical interaction and electrical tunneling between adjacent aggregates that are in nominal contact. As the composite is stretched, the percolative network degrades and the bulk electrical resistance increases significantly [29]. Moreover, due to inelasticity from internal friction, creep, and relaxation, the conductivity exhibits significant hysteresis between mechanical loading and unloading. [30]. In general, resistive sensing is challenging on account of electromechanical hysteresis and the contributions of contact and lead resistance, which can fluctuate under active loading or during passive motion.

Despite the challenges of soft-matter resistive sensing, there have been several attempts with applications to wearable computing and robotics. Lorussi *et al* used CB–PDMS as strain sensors for a data glove capable of hand posture and gesture monitoring [31]. Recently, Yildiz *et al* [32] presented fabrication and characterization of highly stretchable elastomeric resistive strain sensors with liquid conductors. More recently, Giffney *et al* presented sensing composites using multi-walled carbon nanotubes in a silicone rubber matrix [33]. However, these work focused on stand-alone sensor properties and did not demonstrate the integration of sensors into a robot hand.

Unlike resistive sensors, soft-matter capacitors are robust to electrical hysteresis and fluctuations in lead resistance. Several recent efforts have explored the use of capacitive sensing for wearable computing and data gloves. This includes an elastomer-based electronic skin with gold electrodes for monitoring finger articulation with capacitive sensors to detect pressure [34]. Markvicka *et al* used CB-filled polyacrylate elastomer as soft capacitive electrodes in a stick-on ‘data skin’ for gesture monitoring [35]. In this study, we build on this work by extending the use of soft-matter capacitors to sensing in a prosthetic hand.

3. Materials and methods

3.1. Sensor fabrication

Polydimethylsiloxane (PDMS) (Sylgard 184, Dow Corning) was used as the base material and structured carbon black (Alfa Aesar) was used as the filler for the conductive CB–PDMS composite. The conductivity of CB–PDMS is controlled by physical contact or tunneling between CB aggregates and can be modeled using percolation theory [36, 37]. To ensure proper conductivity, the sensors were made with a relatively high concentration of (25% by wt%) of CB. While percolation can be achieved with a lower concentration (~ 12 wt%), a 25% weight fraction allows for more percolating pathways and greater volumetric conductivity. The composite is prepared by shear mixing the CB powder with uncured PDMS and adding an equal weight of hexane in order to reduce

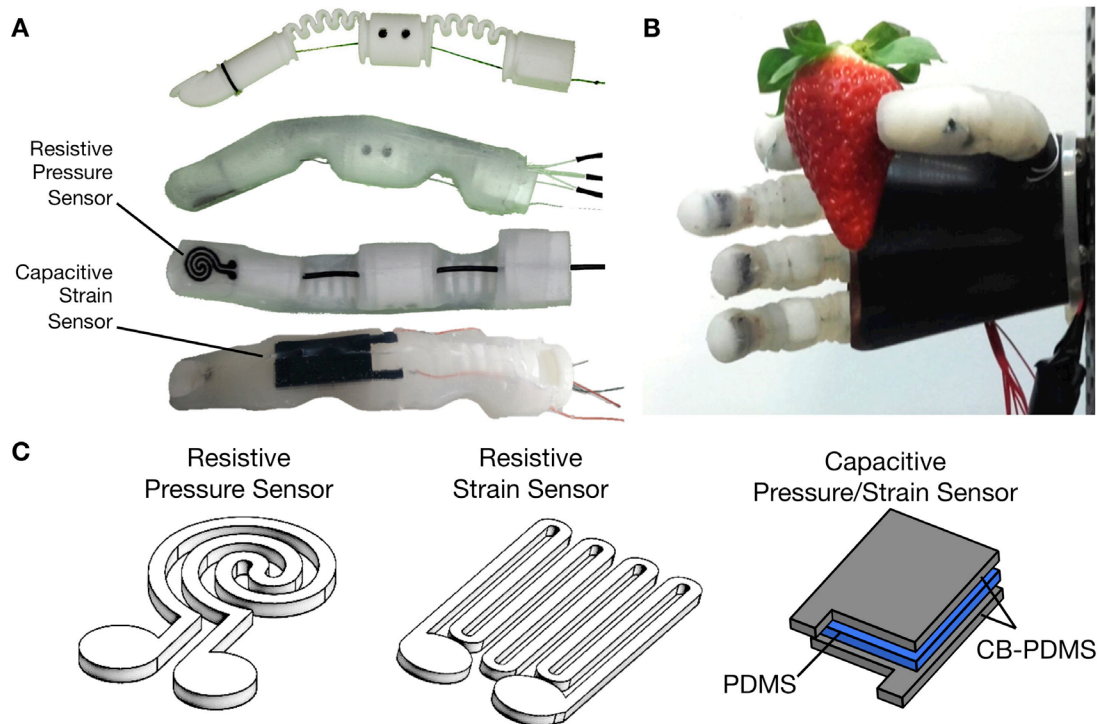


Figure 1. ((A) and (B)) Resistive sensor mounted to the fingertips of a soft robot hand prosthetic. (C) Schematics of the resistive and capacitive sensors.

viscosity and improve the CB dispersion. The composition is mixed with a magnetic stirrer for 4 h, during which time the hexane evaporates.

To produce the sensors, stencil-based lithographic patterning was employed. Masks were cut with a CO₂ laser engraver (VLS 3.50; Universal Laser Systems, Inc.) and placed over a cured sheet of PDMS. Next, the CB-PDMS was deposited over the mask using a thin film applicator (ZUA 2000 Universal Applicator; Zehntner), which ensured a 500 μm thick layer of conductive material. The stencil was then removed and the CB-PDMS is cured on a hot plate for 10 min at 120 °C. After that, a second layer of PDMS was poured over the CB-PDMS. In the case of capacitive sensors, additional layers of CB-PDMS and PDMS were deposited to create alternating insulating and conductive layers [38].

Referring to figure 1(C), we developed resistive and capacitive sensors for measuring either strain or pressure. Strain sensors are used to measure the bending angle of the joints and pressure sensors are placed on the fingerprint to detect touch. For resistive sensors, a spiral geometry proved to be more sensitive for a pressure sensor, while a serpentine geometry is better suited for a strain sensor. For the capacitive sensors, the electrodes are simple rectangles with different sizes to fit in the back of the finger (strain sensor) or on the fingerprint (pressure sensor).

3.2. Finger design and fabrication

Inspired by the human finger, the soft finger is composed of three layers: (i) an internal rigid endoskeleton similar to the human bone (3D printed from Nylon powder in ShapeWays with selective laser sintering process), (ii) a soft silicone layer

similar to the human dermal layer (EcoFlex Gel, Smooth On), and (iii) a dermal layer (EcoFlex 0030, Smooth On). Thin sensors are implanted between the dermal and epidermal layers. The 3D printed endoskeleton is composed of compliant joints, with compliance that depends on the geometry of the joint. The choice of design parameters for the anthropomorphic finger is explained in [15].

The artificial finger was produced using an SDM approach in which the 3D printed endoskeleton was fixed inside of a mold that was then filled with uncured silicone (Ecoflex; Smooth-On). This requires an intermediate step in order to integrate the sensors, electrical wiring, and actuator cables. Two different molds were thus designed and built to accommodate fabrication: the intermediate mold with flat surfaces in specific regions to make it easier to place the sensors and the final mold for the finger's final shape. Before casting the finger with the intermediate mold, the string responsible for the finger's bending motion had to be run across the channels that go through the endoskeleton (see figure 1(A)). This was simply achieved by securing one end of the string near the beginning of the nail and sliding the other end across the channels in the 3D printed mold. The main issue was how to keep the silicone from permeating the fibers of the string. Preliminary tests showed that the force needed to bend the finger greatly increased if the string was not properly protected. Therefore, before inserting the string, we first surrounded it with a 1.6 mm, 2:1 ratio thermo-retractable sleeve to isolate it. After insertion of the sleeve, we were able to guide the cabling through the embedded channels.

The inner skin's design was based on the following different guidelines: create two flat regions, one at back of the finger and another one below the fingertip, with enough space

to place the sensors, while at the same time trying to minimize the volume around the remaining regions of the finger in order to keep the final finger from becoming too thick. This geometry is suitable not only to properly place the sensors but also to integrate the electrical wires. The intermediate mold was then created from this skin model, split into two symmetric halves and 3D-printed using polylactic acid (PLA). The mold also accommodates some added holes to allow the injection of Ecoflex and release of air, a support for it to stand, and a cavity/protrusion system to align both halves and a inner channel for the thermo-retractable sleeve to pass through. Once printed, each side wall of the mold was pierced by two screws in order to better secure and center the endoskeleton within the mold. The mold was then tightly closed and casted with Ecoflex. After this stage the sensors and the electrical wires were integrated. Each flat surface was first brushed with uncured Ecoflex which, once cured, acted as a bonding agent between the inner skin and the sensors. As to the electrical wires, these were integrated by simply sewing the wires along the sides of the inner skin with the help of a very thin needle. There are four wires in total, two for each sensor, with each one being connected to a sensor pad.

3.3. Sensor-finger integration

The mold for the final finger is designed in order to completely cover the inner skin, sensors, and wires while at the same time resembling a normal human finger as much as possible. This meant that the model could not be excessively thick and had to guarantee a continuous and well covering skin. Moreover, previous iterations of the final design revealed that excess material in the regions beneath the joints caused a buckling effect that greatly increased the force necessary to bend the finger. Just like the intermediate mold, the outer skin mold was split into symmetric halves and complemented with holes for the silicone for the passage of air and Ecoflex, a support, an alignment system and a channel for the retractable sleeve. A screw at each side wall was also added for centering purposes. After casting the final mold with the outer skin material and curing (1 h at room temperature), that remained was to carefully extract the sleeve. The same procedure was also used for integration of the capacitive sensors. Lastly, in order to produce the latest version of the ISR soft bionic hand, five different fingers were developed using the same method described here (figure 1(B)).

3.4. Sensor testing

We characterized the pressure sensors by applying force with an adjustable linear system that allow the user to control the pressure to be applied. Applied force was read using a digital scale beneath the sensor and the resistance or capacitance was acquired by an LCR meter (Iso-Tech, LCR 819). For capacitive pressure sensors, instead of a metal object to press the sensors, it was used a plastic object to avoid interference in the signal. Strain sensors were characterized using a setup in which the sensor was attached to two fixtures connected to

an adjustable linear system. The system could be configured to select the desired strain to apply and the velocity of the loading and unloading.

In order to analyze the electromechanical coupling, two different tests were conducted: (i) loading and unloading characterization and (ii) immediate response after loading. For the loading and unloading test we allowed 45 s between each measurement to allow the sensor to stabilize to eliminate the effect of the viscoelastic behavior of the polymer. On the second test, we continuously monitored the resistance after a stimuli to understand how other parameters such as viscoelasticity of the polymer affects the recovery time.

4. Theoretical modeling

In order to predict the behavior of the sensors, theoretical models for resistive and capacitive strain and pressure sensors were developed. The resistance R of a conductor can be computed as $R_0 = \rho \ell / A$, where ℓ is the length of the conductor, A is the cross section and ρ is the materials specific electrical resistance. To develop an approximate model for R/R_0 , changes in the geometric dimensions of the conductors due to the application of pressure or strain must first be predicted. Strain sensors comprise a total length, width and thickness of 200 mm, 1 mm, and 500 μm , respectively. For the serpentine geometry, the length is divided into eight strips. Under strain, the length of the sensor is increased while the thickness and width of the conductive traces are reduced. Since the cPDMS is an incompressible material, its Poisson ratio is $\nu = 0.5$. Therefore,

$$\frac{\Delta \ell}{\ell_0} = \varepsilon_\ell = -\nu \varepsilon_w = -\nu \varepsilon_t, \quad (1)$$

where, $\varepsilon_\ell, \varepsilon_t, \varepsilon_w$ are strain in the principal directions. This implies that the relative resistance R/R_0 can be estimated as

$$\frac{R}{R_0} = \frac{1 + \varepsilon_\ell}{(1 - \nu \varepsilon_\ell)^2}. \quad (2)$$

When pressure is applied, the thickness of the traces is reduced, the width increases, and the length remains constant. Based on the Hooke's law, $\sigma = E\varepsilon$, where σ is the applied stress, ε is the strain, and the elastic modulus E varies [39, 40] depending on whether the elastomer is in compression or tension. The relative changes in resistance can be estimated by the following equation:

$$\frac{R}{R_0} = \frac{wt\ell}{(w - \frac{6\nu\sigma w}{E_t})(t - \frac{\sigma t}{E_c})\ell}. \quad (3)$$

The theoretical predictions obtained from this equations are compared with experimental measurements in the Results section.

In the case of capacitive sensing, we estimate the electromechanical response with respect to the natural (unloaded) capacitance $C_0 = \epsilon_0 \epsilon_r A_0 / d_0$ where A_0 is the area of the conductive electrodes, d_0 is the gap, ϵ_0 is the vacuum permittivity, and ϵ_r the dielectric permittivity (2.3–2.8 for PDMS [40], and 4.2 for EcoFlex 0030, [41]). To predict the electromechanical

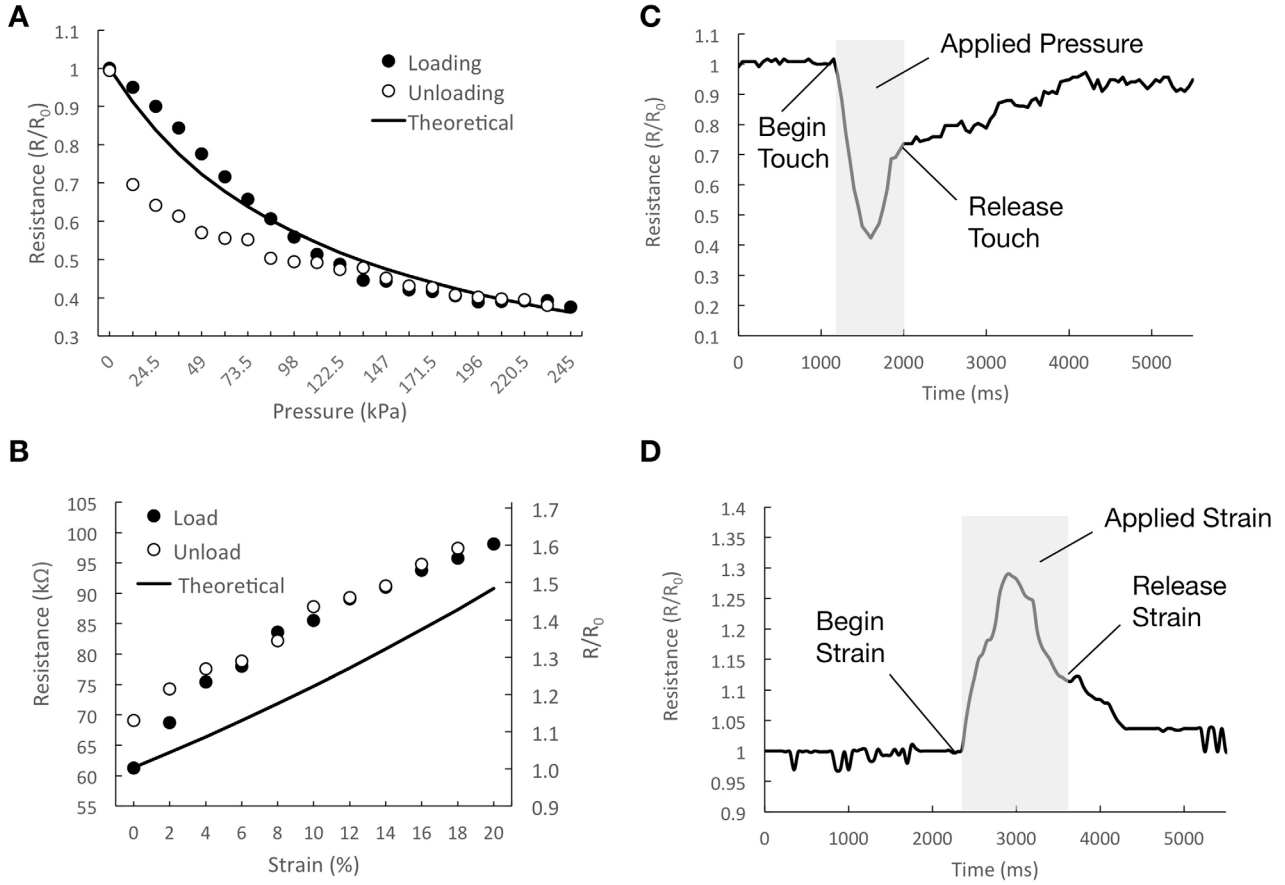


Figure 2. Load and unload cycle of the resistive (A) pressure and (B) strain sensors. Continuous measurement of sensors signals when (C) 250 kPa pressure and (D) 25% strain is applied and then immediately removed.

response under an applied pressure stress σ , we again assume Hooke's Law, which implies that

$$\frac{C}{C_0} = \left\{ 1 - \frac{\sigma}{E} \right\}^{-1}. \quad (4)$$

Lastly, for capacitive strain sensors with an applied strain ε_ℓ , $C/C_0 = 1 + \varepsilon_\ell$.

5. Results

5.1. Resistive sensors

Figure 2 shows the electromechanical response of the resistive pressure and strain sensors. When a compressive stress was applied to the pressure sensor (figure 2(A)), its resistance decreased as expected according to the theoretical prediction from equation (3). However, significant hysteresis is observed, with poor theoretical agreement during the unloading cycle. This is likely due to the large internal stresses and the intrinsic electromechanical hysteresis of the percolating CB network. The strain sensor also exhibited hysteresis, although in this case the theoretical prediction, from equation (2), was in much stronger agreement with the experimental measurements during *unloading*.

One particular problem of the resistive pressure sensor was the recovery time. After unloading, full recovery of the initial resistance value takes over 10 min. Therefore, it was necessary

to allow 20 min before repeating tests on the same sensor. To have a better understanding of the recovery time, we applied a force to the sensors and acquired the resistance of a pressure and strain sensor every 50 ms. In this test, we applied 250 kPa of pressure (figure 2(C)) or 20% strain (figure 2(D)) and then immediately removed it. As the results show, the electrical response is ~ 1 s but the recovery time after the load is removed is ~ 3 s (for a 90% reduction in signal). In general, the recovery time is slow, and in most cases a 100% recovery does not occur which explains the hysteresis.

Both the hysteresis and slow recovery time are likely governed by the degradation of the percolating CB network when the composite is mechanically loaded. Some of the internal conductive pathways immediately recover after load is removed. However, complete stabilization of electrical conductivity takes time (seconds or minutes) due to viscoelasticity and creep. Also some connections between particles are permanently broken due to inelastic deformation. For these reasons, we do not believe that resistive sensing is appropriate in the soft robot prosthetic hand.

5.2. Capacitive sensors

The main advantage of the capacitive sensing is that the capacitance is only dependent on geometry and not on the bulk conductivity of the elastomer. The same set of tests that were performed for resistive sensors were also performed on

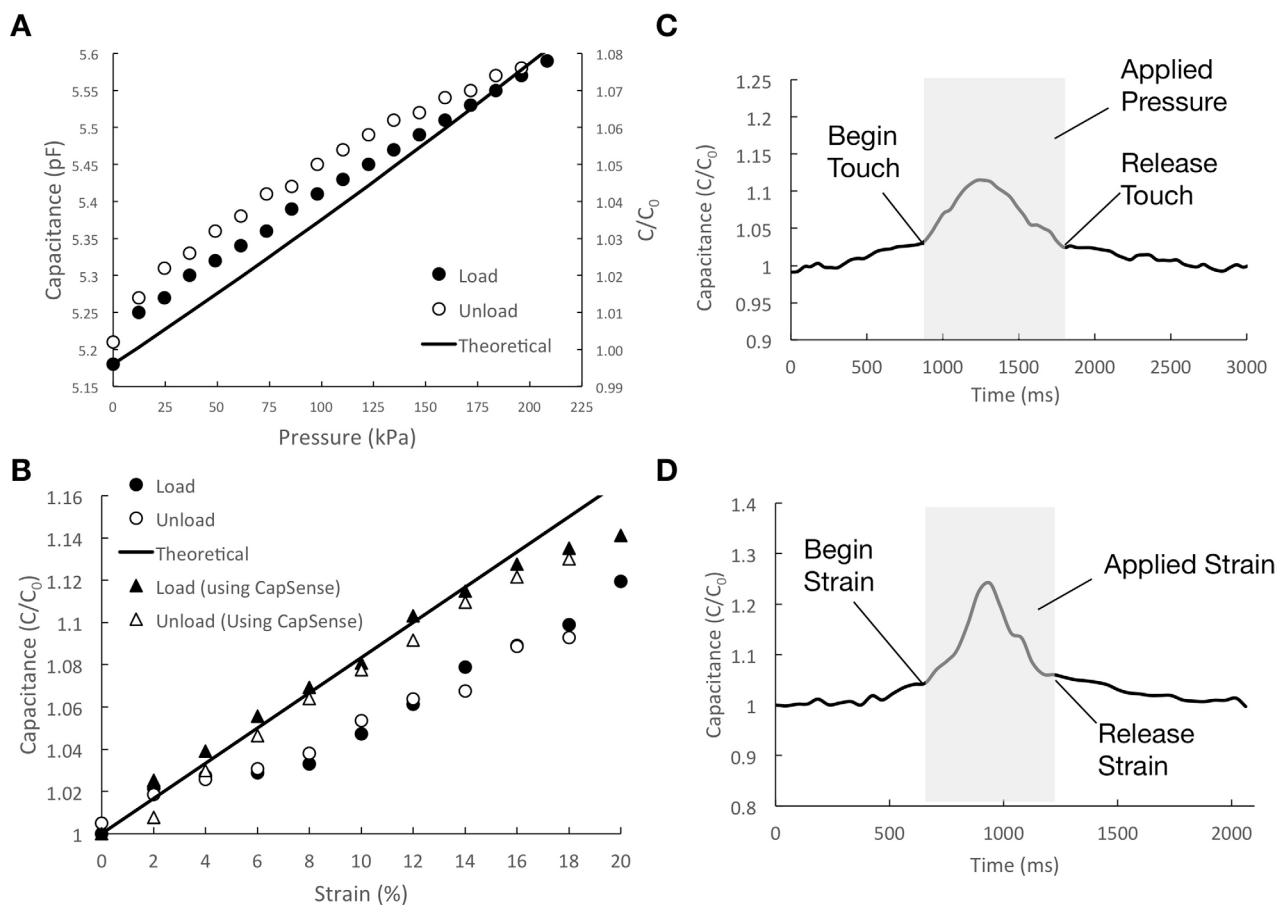


Figure 3. Load and unload cycle of capacitive (A) pressure and (B) strain sensors. Continuous measurement of sensors signals when (C) 250 kPa pressure and (D) 25% strain is applied and then immediately removed.

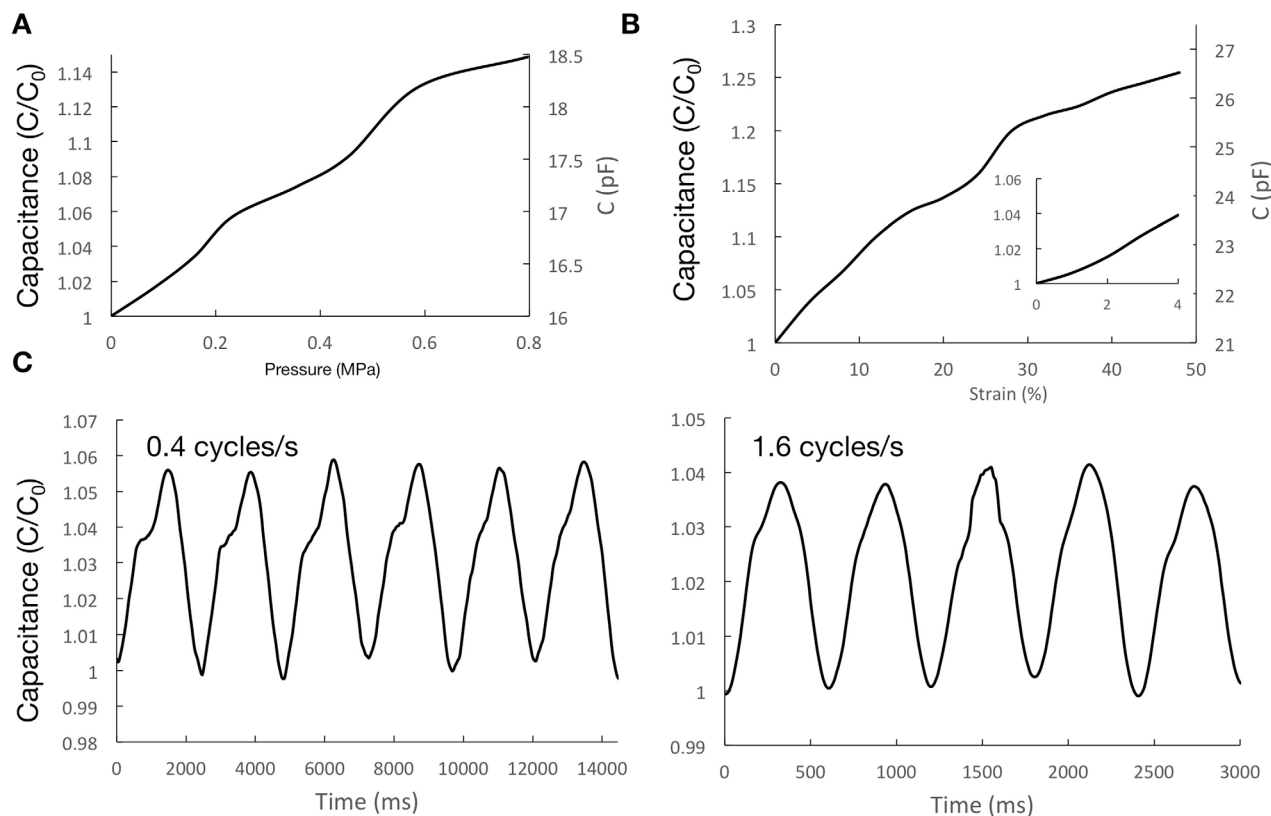


Figure 4. Change in capacitance under a continuous increase in (A) pressure and (B) strain. (C) Change in capacitance under cyclical loading with 20% tensile strain.

capacitive sensors. As can be seen in figures 3(A) and (B), the measured hysteresis is much smaller when compared to the values obtained for the resistive pressure sensors.

The theoretical prediction from equation (4) appears to be in reasonable agreement with experimental measurements of C/C_0 when pressure is applied. We also see good agreement with theory when the capacitive sensor is stretched, although the agreement is much stronger when capacitance is measured using the more sensitive CapSense data acquisition system (cypress semiconductor). We also find a significant improvement in recovery time compared to the resistive sensors. As shown in figures 3(C) and (D), there is almost 100% recovery within seconds of removing the applied mechanical load. Based on these results, capacitive sensing was identified to be more suitable for the soft robot gripper.

Additional characterization was performed using the CapSense acquisition system since it has greater sensitivity than the LCR meter (LCR 819; Iso-Tech) used to collect data in figure 3(A). The system uses a capacitive sigma delta (CSD) sensing algorithm in which capacitive sensing is performed using a switched capacitor technique with a delta-sigma modulator that converts the sensing current to a digital code [42]. First, we analyzed the resolution and the maximum pressure and strain that are detected by the sensors (figures 4(A) and (B)). The maximum pressure that is measurable in the fingertip sensor is 225 kPa, which corresponds to a normal force of 17 N (sensor area = 10 mm × 8 mm). The minimum pressure that the sensor can measure is ~1 kPa and the resolution is approximately 60 Pa of difference (i.e. 4.8 mN of normal force). The strain sensors can measure strain in the range of 1% of 48%, which is limited by the mechanical strain limit of the composite. As shown in figure 4(C), the electro-mechanical response is similar when strained to 20% for 0.4 and 1.6 Hz cyclical loading.

Additionally, the capacitive strain sensor was used as a bend sensor to measure of bending angle in the joint of the robot finger. We made 850 consecutive tests by bending the finger from fully open to fully bent and acquired the data to analyze the repeatability and the drift of the sensor. To perform this test, the setup shown in figure 5(A) was used. The plot in figure 5(A) shows the maximum and minimum of each cycle while figure 5(B) presents the change of capacitance in specific cycles, acquired in the beginning, in the middle and in the end of the session. By comparing the plots, one can verify the repeatability of the sensor and a slight drift on the capacitance from the beginning to the end of the test. Nevertheless $\Delta C = C_{\max} - C_{\min}$ remains approximately constant.

5.3. Mechatronics and data acquisition

Each finger weighs 27 g and the endoskeleton requires 1.8 N to fully bend. The fully integrated finger with the silicone skin requires around 4.6 N to bend until the point at which the fingertip is parallel to the knuckle. Details of the endoskeleton optimization and finger fabrication is described in [15]. To validate the control system, the hand was tested to grasp a strawberry, grape, needle, nut, and pen (figures 1(B) and 6(A)). The hand stops during the closing motion when

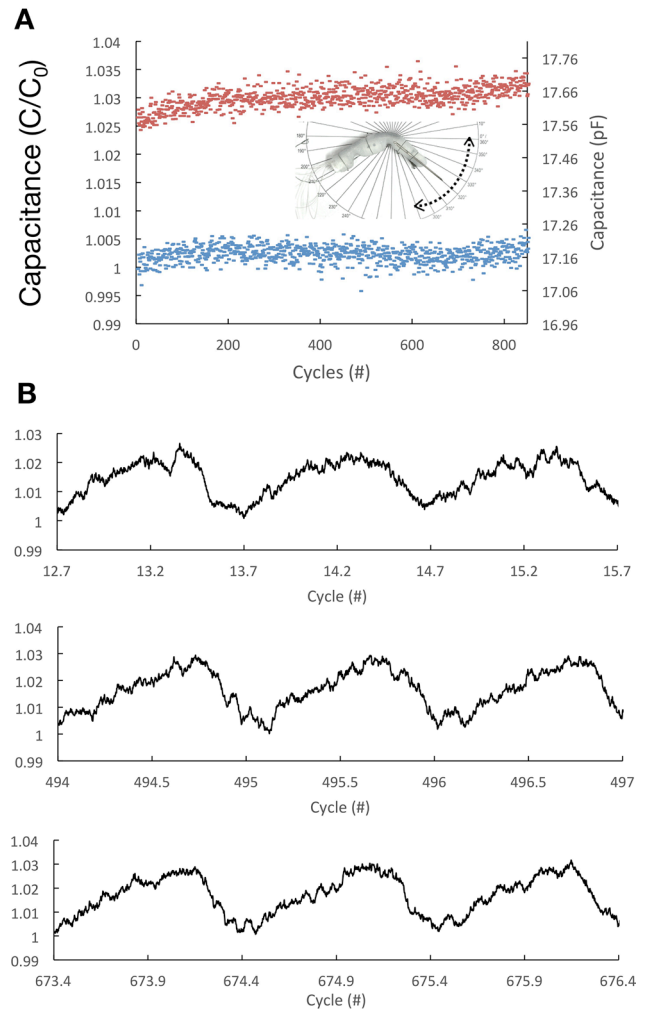


Figure 5. (A) Electromechanical response for 70° bending cycles; (C) electromechanical response at different cycles in the test.

some conditions are satisfied. To verify these conditions an ad-hoc control and measurement board was developed based on the cypress semiconductor CapSense technology. Using this board, by changing the sample number and frequency, we can adjust the sensitivity of the sensor.

5.4. Control of the hand with pressure sensor feedback

While generally reliable, there are some technical limitations with the capacitive sensor. The capacitive sensor is easily interfered when a conductive object or human finger approaches the sensor due to changes in the electric field of the capacitor. To limit the effect of proximity, all wires are shielded. Active shielding consists of using a shielded cable. The shield is then connected to the ‘shield’ pin of the board. While this method is effective in noise reduction, the sensor itself is still sensitive to proximity. When the hand is closing and the sensors are approaching a conductive object, it results in an increase in capacitance (even without touching), which may stop the closing movement. Figure 6(B) shows the changes of capacitance of pressure sensors integrated into the bionic finger, due to proximity and pressure of different objects. As can be seen, when a metal object or a human finger approaches the sensor,

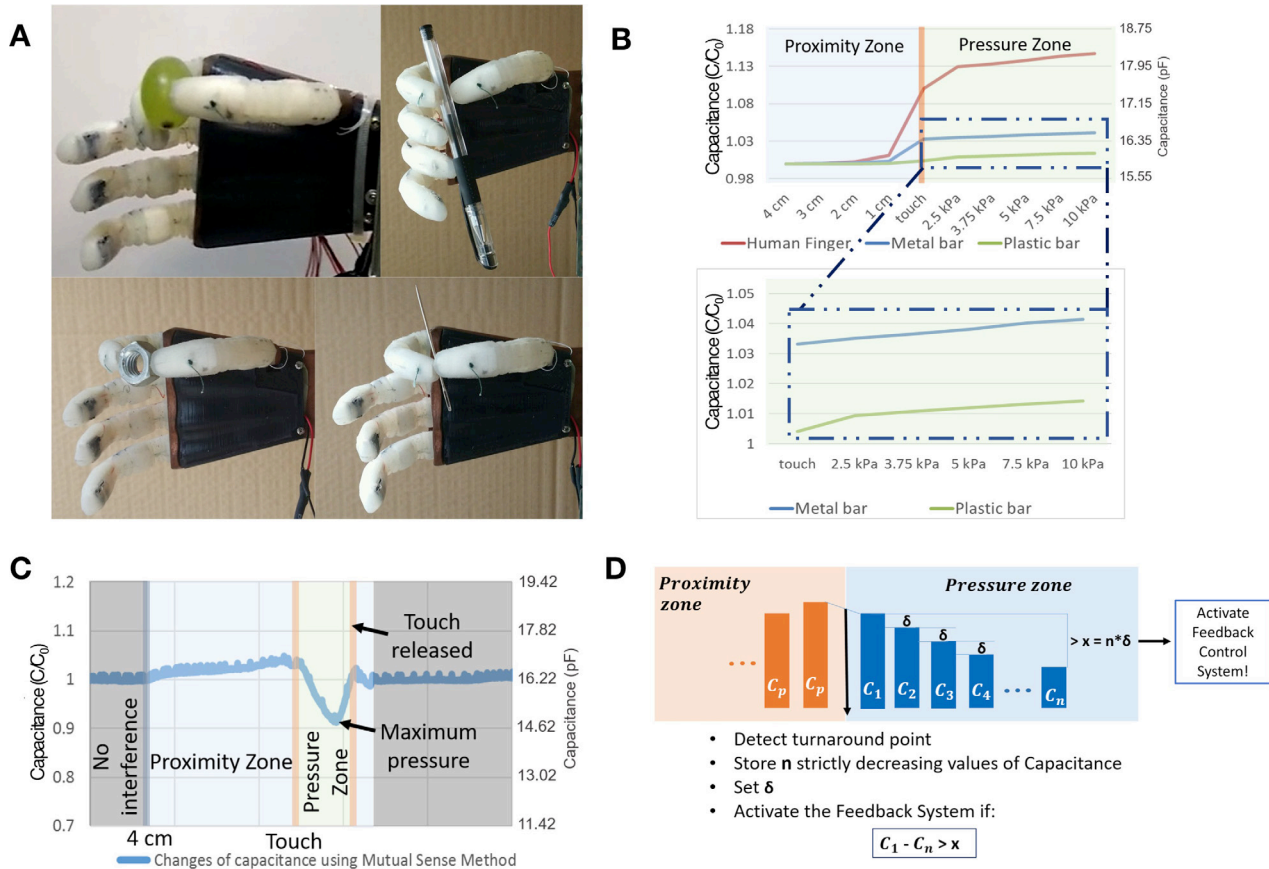


Figure 6. (A) ISR soft bionic hand with integrated sensors grasping various objects. (B) Changes on capacitance with a human finger, a metal object and a plastic object approaching and pressing the sensor from the bionic finger, using the self capacitance sensing method. A close view of the changes when the sensor is pressed by the metal bar and by the plastic bar. (C) Changes on capacitance with a metal object approaching and pressing the finger, using the Mutual sensing method. (D) Schematic of the algorithm used for the control system of the hand. When an object touches the sensor, the capacitance counts start to decrease. Therefore, this turnaround point is detected and then a strictly decreasing behavior of, at least, five values is stored to verify if the threshold of pressure x is reached. If the threshold is achieved, the pulling of the hand tendons is stopped.

the feedback system would stop the closing movement, even without touch.

To distinguish between proximity and contact, we use two different of capacitive sensing modes: self capacitance and mutual capacitance. The first one consists of using one of the electrodes connected to the ground. This sensing system operates by driving current on a pin connected to a sensor and measuring the voltage. This method enhances the proximity detection. In the other method, one electrode is used as the receiver and the other as transmitter. The transmitter electrode is driven with voltage pulses, synchronized at a determined frequency, which injects current into the receiver electrodes' capacitance through the mutual capacitance between both electrodes. Using this mutual capacitance method, the proximity and pressure have different effects on the sensor capacitance, as is shown in figure 6(C). Therefore, although the proximity of a conductive object causes an increase in the capacitance counts from CapSense, when the object touches the bionic finger and presses the sensor, the capacitance starts to decrease [43]. In mutual capacitance sensing method, the approach of an object, causes a redistribution of charges which result in an increase in the capacitance counts until touch occurs. This is represented by the proximity zone in figure 6(C). When touch occurs, the capacitance counts starts

to decrease, as shown in the 'pressure zone'. Such response is the opposite to what happens in a self capacitance method (see figure 6(B)). The turnaround points, marked with the orange bars, are the instants when the touch is applied and released. Therefore, we can distinguish between proximity and touch. In this case, the algorithm depicted in figure 6(D) can be used. In this algorithm, when the turnaround point of the capacitance is detected (i.e. contact is made), the capacitance counts of all sensors are acquired and stored on an array with dimension n . In addition to the measurement of pressure, it is important for the control loop of the hand to reliably detect the beginning of touch. In order to disregard the noise, a strictly decreasing behavior, where the actual reading of capacitance should be lower than the previous value by δ for n cycles (e.g. 5 cycles), is considered as the threshold to detect the pressure. Otherwise, the values stored in the array are deleted and the system starts again. With this clause, the noise from spontaneous increase or decrease of capacitance counts due to movement or other interference is filtered out. When the pressure causes the capacitance to reach a predefined threshold, ' x ', calculated by the difference between the first and the last value of the array, the hand's actuators stop pulling the tendons. The definition of x gives the sensitivity of the system and can be adjusted for different objects.

6. Conclusions

In this article, we demonstrated fabrication, characterization and integration of a low-cost soft bionic finger with embedded pressure and bend sensors made of conductive elastomer. By using materials and fabrication equipment that are readily accessible and inexpensive, the fingers can be replicated or customized by a broad community of users. Since they are composed of soft silicone, sensors can be seamlessly integrated into the soft skin of the hand without altering its ability to conform to objects.

Theoretical predictions for both resistive and capacitive sensing are compared to experimental measurements. In general, the theory and experiment are in reasonable agreement, although data fitting is used for some of the comparisons. Electromechanical hysteresis and recovery time under pressure and tensile loading are measured for both type of sensors. From these measurements, we conclude that resistive sensors made with CB-PDMS are not appropriate options neither for pressure sensing nor as a strain/bending sensors due to their high hysteresis and slow recovery time. Instead, capacitive sensors are more robust to transient loading effects. One associated problem with the capacitive sensor is the proximity of human fingers or conductive objects to the sensors, which can increase the capacitance and might be interpreted as a touch event. However, this can be addressed by adopting a mutual capacitance sensing method, which allows for distinguishing between proximity and touch.

Acknowledgments

This work was supported by the Portuguese Foundation of Science and Technology and the CMU-Portugal program, under the contract number CMUP-ERI/TIC/0021/2014.

Multimedia extension

The video shows a soft prosthetic hand with integrated capacitive sensors, grasping several objects and the effect of proximity and touch of multiple objects on the capacitance of the finger tip sensors are as well presented (stacks.iop.org/JMM/28/034001/mmedia).

ORCID iDs

Rui Pedro Rocha  <https://orcid.org/0000-0002-6160-4858>
 Mahmoud Tavakoli  <https://orcid.org/0000-0002-2590-2196>
 Carmel Majidi  <https://orcid.org/0000-0002-6469-9645>

References

- [1] Castellini C and van der Smagt P 2013 Evidence of muscle synergies during human grasping *Biol. Cybern.* **107** 233–45
- [2] Santello M, Baud-Bovy G and Jörntell H 2013 Neural bases of hand synergies *Front. Comput. Neurosci.* **7** 23
- [3] Catalano M, Giorgio G, Serio A, Farnioli E, Piazza C and Bicchi A 2012 Adaptive synergies for a humanoid robot hand *IEEE-RAS Int. Conf. on Humanoid Robots*
- [4] Bicchi A, Gabbicini M and Santello M 2011 Modelling natural and artificial hands with synergies *Phil. Trans. R. Soc. B* **366** 3153–61
- [5] Godfrey S, Ajoudani A, Catalano M, Grioli G and Bicchi A 2013 A synergy-driven approach to a myoelectric hand *IEEE Int. Conf. on Rehabilitation Robotics* (IEEE) pp 1–6
- [6] Godfrey S B, Bianchi M, Zhao K, Catalano M, Breighner R, Theuer A, Andrews K, Grioli G, Santello M and Bicchi A 2017 The soft-hand pro: translation from robotic hand to prosthetic prototype *Converging Clinical and Engineering Research on Neurorehabilitation II* (Berlin: Springer) pp 469–73
- [7] Tavakoli M and de Almeida A T 2014 Adaptive under-actuated anthropomorphic hand: Isr-soft-hand *IEEE Int. Conf. on Robotics and Automation* (Chicago: IEEE)
- [8] Deimel R and Brock O 2016 A novel type of compliant and underactuated robotic hand for dexterous grasping *Int. J. Robot. Res.* **35** 161–85
- [9] Melchiorri C, Palli G, Berselli G and Vassura G 2013 Development of the UB hand IV, overview of design solutions and enabling technologies *IEEE Robot. Autom. Mag.* **20** 72–81
- [10] Tavakoli M, Marques L and de Almeida A T 2013 Flexirigid a novel two phase flexible gripper *IEEE/RSJ Int. Conf. on Intelligent Robots and Systems* (IEEE) pp 5046–51
- [11] Dollar A M and Howe R D 2010 The highly adaptive sdm hand: design and performance evaluation *Int. J. Robot. Res.* **29** 585–97
- [12] Odhner L, Jentoft L, Clafée M, Corson N, Tenzer R, Ma Y, Buehler M, Kohout R, Howe R and Dollar A 2014 A compliant, underactuated hand for robust manipulation *Int. J. Robot. Res.* **33** 736–52
- [13] Manti M, Hassan T, Passetti G, DELia N, Laschi C and Cianchetti M 2015 A bioinspired soft robotic gripper for adaptable and effective grasping *Soft Robot.* **2** 107–16
- [14] Tenzer Y, Jentoft L P and Howe R D 2014 The feel of mems barometers: inexpensive and easily customized tactile array sensors *IEEE Robot. Autom. Mag.* **21** 89–95
- [15] Tavakoli M, Sayuk A, Lourenco J and Neto P 2017 Anthropomorphic finger for grasping applications: 3D printed endoskeleton in a soft skin *Int. J. Adv. Manuf. Technol.* **91** 2607–20
- [16] Hammock M L, Chortos A, Tee B C-K, Tok J B-H and Bao Z 2013 25th anniversary article: the evolution of electronic skin (e-skin): a brief history, design considerations, and recent progress *Adv. Mater.* **25** 5997–6038
- [17] Bhandarkar A J and Wang J 2014 Non-invasive wearable electrochemical sensors: a review *Trends Biotechnol.* **32** 363–71
- [18] Honda W, Harada S, Arie T, Akita S and Takei K 2014 Wearable, human-interactive, health-monitoring, wireless devices fabricated by macroscale printing techniques *Adv. Funct. Mater.* **24** 3299–304
- [19] Rogers J A, Someya T and Huang Y 2010 Materials and mechanics for stretchable electronics *Science* **327** 1603–7
- [20] Dickey M D 2014 Emerging applications of liquid metals featuring surface oxides *ACS Appl. Mater. Interfaces* **6** 18369–79
- [21] Cheng S and Wu Z 2012 Microfluidic electronics *Lab Chip* **12** 2782–91
- [22] Nambiar S and Yeow J 2011 Conductive polymer-based sensors for biomedical applications *Biosens. Bioelectron.* **26** 1825–32
- [23] Zhang W, Dehghani A and Blackburn R 2007 Carbon based conductive polymer composites *J. Mater. Sci.* **42** 3408

- [24] Niu X, Peng S, Liu L, Wen W and Sheng P 2007 Characterizing and patterning of PDMS-based conducting composites *Adv. Mater.* **19** 2682–6
- [25] Matsuhisa N, Kaltenbrunner M, Yokota T, Jinno H, Kuribara K, Sekitani T and Someya T 2015 Printable elastic conductors with a high conductivity for electronic textile applications *Nat. Commun.* **6** 7461
- [26] Stoyanov H, Kolloosche M, Risse S, Waché R and Kofod G 2013 Soft conductive elastomer materials for stretchable electronics and voltage controlled artificial muscles *Adv. Mater.* **25** 578–83
- [27] Wang Y et al 2017 A highly stretchable, transparent, and conductive polymer *Sci. Adv.* **3** e1602076
- [28] Ma P, Siddiqui A, Marom G and Kim J 2010 Dispersion and functionalization of carbon nanotubes for polymer-based nanocomposites: a review *Composites A* **41** 1345367
- [29] Knite M, Teteris V, Kiploka A and Kaupuzs J 2004 Polyisoprene-carbon black nanocomposites as tensile strain and pressure sensor materials *Sensors Actuators A* **110** 142–9
- [30] Zhang X-W, Pan Y, Zheng Q and Yi X-S 2000 Time dependence of piezoresistance for the conductor-filled polymer composites *J. Polym. Sci. Part B: Polym. Phys.* **38** 2739–49
- [31] Lorussi F, Scilingo E P, Tesconi M, Tognetti A and De Rossi D 2005 Strain sensing fabric for hand posture and gesture monitoring *IEEE Trans. Inf. Technol. Biomed.* **9** 372–81
- [32] Yildiz S, Mutlu R and Alici G 2016 Fabrication and characterisation of highly stretchable elastomeric strain sensors for prosthetic hand applications *Sensors Actuators A* **247** 514–21
- [33] Giffney T, Bejanin E, Kurian A S, Travas-Sejdic J and Aw K 2017 Highly stretchable printed strain sensors using multi-walled carbon nanotube/silicone rubber composites *Sensors Actuators A* **259** 44–9
- [34] Gerratt A, Michaud H and Lacour S 2015 Elastomeric electronic skin for prosthetic tactile sensation *Adv. Funct. Mater.* **25** 2287–95
- [35] Bartlett M D, Markvicka E J and Majidi C 2016 Rapid fabrication of soft, multilayered electronics for wearable biomonitoring *Adv. Funct. Mater.* **26** 8496–504
- [36] Amnon A and Stauffer D 2010 *Introduction to Percolation Theory* (London: Taylor and Francis) ch 1
- [37] Decrossas E, Sabbagh M, Hanna V and El-Ghazaly S 2012 Formulation based on percolation theory to model the effective conductivity of carbon nanotube networks *IEEE Int. Symp. on Electromagnetic Computability* **2012** 396–400
- [38] Tavakoli M, Rocha R, Osorio L, Almeida M, de Almeida A, Ramachandran V, Arya T, Lu T and Majidi C 2017 Carbon doped PDMS: conductance stability over time and implications on additive manufacturing of stretchable electronics *J. Micromech. Microeng.* **27** 035010
- [39] Wang Z 2011 Polydimethylsiloxane mechanical properties measured by macroscopic compression and nanoindentation techniques *MSc Thesis* University of South Florida
- [40] Mark J 1998 *Polymer Data Handbook* (Oxford: Oxford University Press)
- [41] Maiolino P, Galantini F, Mastrogiovanni F, Gallone G, Cannata G and Carpi F 2015 Soft dielectrics for capacitive sensing in robot skins: performance of different elastomer types *Sensors Actuators A* **226** 37–47
- [42] Cypress SemiConductors 2015 AN64846—Getting Started with CapSense
- [43] PSoC 4 and PSoC Analog Coprocessor CapSense Design Guide, Cypress Semiconductor (<http://cypress.com/file/46081/download>) (Accessed: 1 November 2017)